OXFORD

SOT | Society of Toxicology
www.toxsci.oxfordjournals.org

*TOXICOLOGICAL SCIENCES*, 148(1), 2015, 192–203

doi: 10.1093/toxsci/kfv176
Advance Access Publication Date: August 13, 2015
Research Article

# Gold Nanoparticles Increase Endothelial Paracellular Permeability by Altering Components of Endothelial Tight Junctions, and Increase Blood-Brain Barrier Permeability in Mice

Ching-Hao Li,[*,†] Ming-Kwang Shyu,[‡] Cheng Jhan,[§] Yu-Wen Cheng,[¶] Chi-Hao Tsai,[§] Chen-Wei Liu,[§] Chen-Chen Lee,[||] Ruei-Ming Chen,[†,|||,||||] and Jaw-Jou Kang[§,1]

[*]Department of Physiology, School of Medicine, College of Medicine, Taipei Medical University, Taipei, Taiwan; [†]Graduate Institute of Medical Sciences, College of Medicine, Taipei Medical University, Taipei, Taiwan; [‡]Department of Obstetrics and Gynecology, National Taiwan University Hospital, Taipei, Taiwan; [§]Institute of Toxicology, College of Medicine, National Taiwan University, Taipei, Taiwan; [¶]School of Pharmacy, Taipei Medicine University, Taipei, Taiwan; [||]Department of Microbiology and Immunology, School of Medicine, China Medicine University, Taichung, Taiwan; [|||]Cell Physiology and Molecular Image Research Center, Taipei Medical University's Wan-Fang Hospital, Taipei, Taiwan; and [||||]Anesthetics Toxicology Research Center, Taipei Medical University Hospital, Taipei, Taiwan

[1]To whom correspondence should be addressed at Institute of Toxicology, College of Medicine, National Taiwan University, 1 Jen-Ai Road, Section 1, Taipei 100, Taiwan. Fax: +886-2-23410217. E-mail: jjkang@ntu.edu.tw



## ABSTRACT

Gold nanoparticles (Au-NPs) are being increasingly used as constituents in cosmetics, biosensors, bioimaging, photothermal therapy, and targeted drug delivery. This elevated exposure to Au-NPs poses systemic risks in humans, particularly risks associated with the biodistribution of Au-NPs and their potent interaction with biological barriers. We treated human umbilical vein endothelial cells with Au-NPs and comprehensively examined the expression levels of tight junction (TJ) proteins such as occludin, claudin-5, junctional adhesion molecules, and zonula occludens-1 (ZO-1), as well as endothelial paracellular permeability and the intracellular signaling required for TJ organization. Moreover, we validated the effects of Au-NPs on the integrity of TJs in mouse brain microvascular endothelial cells *in vitro* and obtained direct evidence of their influence on blood-brain barrier (BBB) permeability *in vivo*. Treatment with Au-NPs caused a pronounced reduction of PKCζ-dependent threonine phosphorylation of occludin and ZO-1, which resulted in the instability of endothelial TJs and led to proteasome-mediated degradation of TJ components. This impairment in the assembly of TJs between endothelial cells increased the permeability of the transendothelial paracellular passage and the BBB. Au-NPs increased endothelial paracellular permeability *in vitro* and elevated BBB permeability *in vivo*. Future studies must investigate the direct and indirect toxicity caused by Au-NP-induced endothelial TJ opening and thereby address the double-edged-sword effect of Au-NPs.

**Key words**: endothelial barrier; paracellular permeability; tight junction; protein kinase C zeta (PKCζ); blood-brain barrier

## Abbreviations:

AJ, adherens junction;
Au-NPs, gold nanoparticles;
Au-MPs, gold microparticles;
BBB, blood-brain barrier;
BMECs, brain microvascular endothelial cells;
HUVECs, human umbilical vein endothelial cells;
JAMs, junctional adhesion molecules;
MMP, matrix metalloproteinase;
PKC, protein kinase C;
TEER, trans-endothelial electrical resistance;
TEM, transmission electron microscopy;
TJ, tight junction;
VE-cadherin, vascular endothelial cadherin;
ZO-1, zonula occludens-1.

Tight junctions (TJs) are junctions formed between 2 adjacent cells that are responsible for regulating the permeation of polar solutes through the intercellular cleft (the so-called paracellular permeability or barrier function) (Abbott, 2013). TJs are present in both the epithelium and the endothelium. Whereas TJs are concentrated on the apical side of epithelial cells, in endothelial cells, the localization of TJs is intermingled with that of other junctions. Moreover, TJ organization or tightness varies considerably along the vascular tree: it is well developed in arteries/arterioles and loosely elaborated in capillary venules. An exception is the cerebral capillary, where TJs contribute to the blood-brain barrier (BBB): TJs of brain microvascular endothelial cells (BMECs) are tighter than those of peripheral microvessels (Bazzoni and Dejana, 2004). The brain in all vertebrates contains a BBB composed mainly of endothelial cells, astrocytes (as well as their basement membranes), and pericytes (Abbott *et al.*, 2006; Engelhardt and Sorokin, 2009). These "neurovascular units" are considered to constitute the physical barrier of the BBB, which restricts paracellular diffusion of water-soluble substances from blood to brain and maintains brain homeostasis (Abbott, 2013). Current studies on the BBB widely use *in vitro* BBB models prepared using nonBBB endothelium-originated cells [eg, human umbilical vein endothelial cells (HUVECs), which retain TJ-expressing phenotypes and paracellular permeability characteristics] (Beese *et al.*, 2010; Liu *et al.*, 2009).

Structurally, TJs are formed by numerous transmembrane proteins [eg, occludin, claudins, and junctional adhesion molecules (JAMs)], which seal the paracellular cleft by locally dimerizing with each other. The cytoplasmic domains of these transmembrane proteins bind to adaptor proteins such as zonula occludens-1 (ZO-1), and these adaptors mediate the anchorage of the membranous TJ components to actin microfilaments and thereby stabilize the TJ structure (Bazzoni and Dejana, 2004). Consequently, TJ disassembly results not only from a reduction in the expression of transmembrane TJ proteins, but also from a dislocation of ZO-1 from the cell border (Chen *et al.*, 2009; Elias *et al.*, 2009) and this can be reflected by a decrease in the *trans*-endothelial electrical resistance (TEER) or an increase in paracellular permeability (McLaughlin *et al.*, 2004). Besides TJs, the ubiquitously distributed adherens junctions (AJs) also mediate cell adhesion and paracellular permeability. The transmembrane protein vascular endothelial cadherin (VE-cadherin) is the most important component of endothelial AJs. VE-cadherin binds through its cytoplasmic tail to β-catenin, which in turn links to α-catenin and anchors the AJ complex to the cytoskeleton. VE-cadherin overexpression reduces cell proliferation and paracellular permeability, but enhances cell adhesion and migration (Bazzoni and Dejana, 2004; Harris and Nelson, 2010; Taddei *et al.*, 2008).

The integrity of TJs is regulated by various signaling factors, among which the protein kinase C (PKC) family, a group of membrane-associated protein kinases, is considered to be the most common regulator (Rao, 2009; Stamatovic *et al.*, 2006; Willis *et al.*, 2010). At least 12 PKC isozymes have been identified to date, and these can be classified into 3 categories (classical, novel, and atypical) based on their cofactor requirements (Willis *et al.*, 2010). In endothelial cells, inflammatory stimuli frequently induce a large increase in PKCα activity, which results in a loss of the ability of TJs to form a tight barrier (He *et al.*, 2012). Conversely, PKCζ is continuously active under basal resting conditions at least in certain cell types, and PKCζ is the only PKC isoform located at the cell border (Mayanglambam *et al.*, 2011; Newton, 2010). Furthermore, PKCζ has been shown to be a part of the ZO complex, where it is the main kinase that phosphorylates occludin on threonine or tyrosine/serine residues, which determines the assembly or disassembly process of TJs, respectively (Dodane and Kachar, 1996; Jain *et al.*, 2011; Zyrek *et al.*, 2007). Thus, the effects of PKCζ inhibition on TJ organization remain debated.

Gold (Au) in its bulk form is inert, weakly toxic, and biocompatible with various tissues, and gold compounds have long been used for medical purposes. Thus, gold nanoparticles (Au-NPs) are also considered to be highly suitable for application in, for example, cosmetics, biosensors, bioimaging, photothermal therapy, and targeted drug delivery (Khlebtsov and Dykmana, 2011; Panyala *et al.*, 2009). However, the toxicity of several nontoxic or weakly toxic bulk materials increases when the sizes of these materials are reduced to the nanoscale. This increase in toxicity might result from the unique toxicokinetic profiles of nanoparticles, as well as from the ability of the particles to overcome cell barriers. Given the continued increase in the applications of Au-NPs, concerns regarding human safety have received progressively more attention, but how Au-NPs affect BBB permeability has remained poorly studied. Thus, in this study, our aim was to elucidate the interactions of Au-NPs with endothelial cells and barriers composed of endothelial cells. We determined that Au-NP exposure reduced PKCζ phosphorylation and PKCζ-dependent threonine phosphorylation on ZO-1 and occludin, and impaired ZO-1/occludin interaction, and that this was followed by an enhancement of TJ protein degradation and paracellular permeability.

## MATERIALS AND METHODS

*Chemicals.* An uncoated Au-NP aqueous suspension (10 mg/ml) was purchased from LiHo Chem Inc. (Taoyuan, Taiwan). Gold microparticles (Au-MPs) (Sigma-Aldrich, St. Louis, MO; 326585) were chosen as a reference control. All chemicals, unless otherwise indicated, were obtained from Sigma-Aldrich. The chemical stocks of MG-132 and Go6983 were prepared in dimethyl sulfoxide (DMSO). For solvent control, the maximal final concentration of DMSO in the medium was 2‰ (*in vitro* study), and this did not adversely affect cell viability and paracellular permeability.

*Au-NP characterization.* The morphology, particle size, and agglomeration of the gold particles were measured by using transmission electron microscopy (TEM). A drop of the nanoparticle suspension was allowed to air-dry onto a Formvar-carbon-coated 200 mesh copper grid, and then TEM images were acquired on a JEM-2100 microscope operating at 120 kV (JEOL

Ltd., Tokyo, Japan). Approximately, 200 particles were counted and measured for size distribution (AnalySIS software, Soft Imaging Systems, Megaview III, Munster, Germany). The particle size distribution of gold particles was measured in PBS (137 mM NaCl, 2.7 mM KCl, 10 mM $Na_2HPO_4$, 1.8 mM $KH_2PO_4$, pH 7.4) and cell culture medium by dynamic light scattering (DLS) method (Zetasizer 300, Malvern, UK). Furthermore, the zeta potential of the gold particles was measured by laser Doppler velocimetry at a constant temperature of 25°C in the same device. The absorption spectra of gold particles were recorded by using an ultraviolet-visible spectrophotometer (OPTIZEN; Mecasys Co., Ltd., Korea) at the wavelength range 400–800 nm, and sterile water was used as a standard for background correction.

*Primary endothelial cell (HUVEC and BMEC) isolation, culture, and treatment.* Primary vascular endothelial cells derived from distinct donors were isolated from human umbilical cords by means of 0.1% collagenase digestion (for detailed information, please see the Supplementary Information). Primary cultures were grown in a humidified 5%-$CO_2$ atmosphere at 37°C in an incubator, and passages between 3 and 6 were used in the experiments. Culture medium was refreshed every 2 days. Confluent monolayers of HUVECs were treated with gold particles at indicated periods, and subjected to TJ protein (or mRNA) analysis. For paracellular permeability and TEER assays, postconfluent cells were incubated for 2–3 more days after cells had reached confluence.

BMEC cultures were prepared by a modification of Bowman *et al.*'s method (1983) (for detailed information, please see the Supplementary Information). Cell culture protocol for human brain malignant glioma (GBM 8401) and human colonic adenocarcinoma cell lines (Caco-2 and HCT-116) were also addressed in the Supplementary Information.

*Determination of cell viability: MTT assay.* Cell viability was evaluated based on the reduction of 3-(4,5-dimethyl-2-thiazolyl)-2,5-diphenyl-2H-tetrazolium bromide (MTT).

*Immunofluorescent staining of TJ markers.* HUVECs were grown on glass cover slips and treated as indicated for various experiments. After treatment, the cells were fixed using 4% paraformaldehyde, permeabilized with 0.1% Triton X-100 for 5 min at room temperature, and incubated with blocking serum for 30 min. Next, the cells were incubated overnight (4°C) with a primary ZO-1 antibody (1:100; Invitrogen, Camarillo, California; Catalog #40-2200) and then with a fluorescein isothiocyanate (FITC)-conjugated secondary antibody (1:1000 dilution) at room temperature for 1 h in the dark. Lastly, nuclei were counterstained with Hoechst 33342 (5 μM, Molecular Probes, Eugene, Oregon) for 5 min and the samples were washed thrice and then mounted on slides. Fluorescent images were captured by using a Nikon MICROPHOT-FXA camera equipped with Media Cybernetics Image-Pro Express software.

*Analysis of endothelial paracellular permeability in vitro by using FITC-dextran.* The *in vitro* barrier permeability was determined by measuring the transendothelial passage of water-soluble tracers from the apical to the basolateral compartment (Beese *et al.*, 2010; Liu *et al.*, 2009). To measure paracellular permeability, $1 \times 10^5$ HUVECs were seeded on fibronectin-pre-coated Transwell inserts (pore size, 0.4 μm) (Corning, Cambridge, Massachusetts) and cultivated for 2–4 days until a postconfluent cell monolayer was formed. We treated the cultures with Au-NPs for 24 h and then added 200 μg/ml FITC-coupled dextrans (molecular mass, 40 or 70 kDa) into the inner chamber; 30 min later, we measured the concentrations of FITC-dextran in the outer chamber at 485/535 nm (Abs/Em) by using a Paradigm Multi-Mode Plate Reader (Beckman Coulter Inc., Brea, California).

*Measurement of TEER.* HUVECs were seeded at $1 \times 10^5$ cells in 0.3 $cm^2$ polyethylene terephtalate membrane inserts with 0.4 μm pore size (Falcon, Catalog No. 353095) and cultivated for 2–4 days as described previously. After treatment with gold particles, the TEER was measured using an EVOM Epithelial Voltohmmeter (World Precision Instruments; Sarasota, Florida). The normalized TEER values were corrected for background resistance of the culture insert and medium, and expressed as $\Omega \cdot cm^2$.

*Analysis of TJ protein expression and PKCζ phosphorylation: Western blotting.* Confluent cells grown on 60-mm dishes were treated with gold particles for 12–48 h (for TJ protein analysis) or 10–60 min (for PKCζ phosphorylation analysis). Subsequently, cells were washed twice with ice-cold PBS and scraped using 200 μl of RIPA buffer (Li *et al.*, 2012). The samples were centrifuged at 14 000× g for 20 min at 4°C, and the supernatants were collected and used as total cell lysates. Protein concentrations were determined using Bradford reagent, and the lysates were then mixed fully with a ×4 sample buffer; next, proteins (60 μg/lane) were resolved by means of SDS-PAGE and electrotransferred onto PVDF membranes (Millipore, Bedford, Massachusetts). The membranes were blocked using TBST containing 5% skim milk (and, if necessary, the membranes were trimmed), and then incubated overnight at 4°C with primary antibodies against β-catenin, JAM-1, claudin-5, PKCα, phospho-PKCα, PKCζ, phospho-PKCζ (Epitomics, Burlingame, California), VE-cadherin (Genetex, Irvine, California), and occludin (Proteintech, Chicago, Illinois). The membranes were next washed in TBST and then incubated for 2 h at room temperature with horseradish peroxidase-conjugated secondary IgGs (1:5000). Finally, blots were developed using enhanced chemiluminescence (Millipore), and images were captured and densitometrically analyzed using the BioSpectrum AC Imaging system (UVP, Upland, California). All values were normalized relative to the control protein. Some of the blots were stripped by using a commercial stripping buffer (Pierce, Rockford, Illinois) and immunoprobed according to the manufacturer's recommendations.

*Characterizing protein-protein interaction in vitro: co-immunoprecipitation.* Whole-cell lysates were pre-cleared by incubating them briefly with protein A magnetic beads (Millipore), and the collected lysates (1 mg) were used in immunoprecipitations: We added 1 μg/ml of the capture antibodies anti-phospho-threonine (anti-p-Thr) (Santa Cruz, Dallas, Texas; sc-5267), anti-occludin (Proteintech; Catalog No. 13 409), or anti-ZO-1 (Epitomics, S1303) and incubated the samples overnight with rotation at 4°C. Next, the samples were mixed with 50 μl of protein A magnetic beads and incubated with agitation for another 2 h. The captured immunocomplexes were precipitated, washed 3 times with RIPA buffer, and mixed with 100 μl of the elution buffer (125 mM Tris, 0.2% SDS, 0.1% Tween-20). Protein samples were electrophoresed on 10% denaturing gels and analyzed as described in the preceding section.

*Analysis of mRNA-expression data of junction-associated proteins: reverse transcription polymerase chain reaction.* Total RNA was isolated by using the TriPure reagent (Roach, Mannheim,

Germany) according to the manufacturer's protocol. Total RNA quality and quantity were assessed using a NanoDrop ND-1000 Spectrophotometer (Thermo, Wilmington, Delaware), and cDNA was synthesized from the total RNA (3 μg) by using M-MLV reverse transcriptase (Epicentre, Madison, Wisconsin) and Oligo ($dT_{16–18}$) primers. Next, the cDNA (2 μl) was amplified using a Taq DNA polymerase mixture with appropriate primer sets (Supplementary Table 1) and the following amplification protocol: denaturation at 95°C for 5 min, followed by 30–35 cycles of denaturation at 95°C for 30 s, annealing at 60°C for 30 s, and extension at 72°C for 30 s, and then a final extension at 72°C for 10 min. The amplification was assessed by separating samples on 1.5% agarose gels and staining with ethidium bromide (Li *et al.*, 2012). The signal intensity was analyzed using a Gel Logic 100 Imaging system (Kodak, Rochester, New York) and mRNA levels were normalized relative to that of the β-actin control.

*Animal husbandry*. All animals were acclimated and housed in the Animal Center of National Taiwan University (NTUAC) (Taipei, Taiwan) according to its standard operation protocol. Animals were handled in all experiments in accordance with the *Guide for the Care and Use of Laboratory Animals* (National Academy of Sciences Press, 1996) and the procedures were approved by the Institutional Animal Care and Use Committee (approval number: LAC-2013-0038).

*BBB permeability assay in vivo: Evans blue extravasation*. We purchased 6-week-old male ICR mice from NTUAC. Before testing, the mice were grouped (5–6 mice/group) and acclimated for 1 week in the housing room. Mice in the test groups were administered Au-NPs (12.5 or 25 mg/kg b.w.) by means of a single intravenous injection through the tail vein; mice in the negative control groups received the vehicle (saline). The mortality and clinical behavior of the animals were observed daily. There were no changes of behaviors or of the numbers of moribund or dead animals that were related to treatment with the test materials. After the treatment (24 or 48 h), BBB permeability was determined based on Evans blue extravasation (Wang *et al.*, 2011). In brief, Evans blue dye (2% in saline) was injected intravenously at a dose of 2 ml/kg, and 2 h after the injection, the animals were killed and perfused with saline to remove intravascular Evans blue dye. Next, the brain was harvested, weighed, and immersed in formamide (10 ml/g) at 55–60°C for 24 h, and then the supernatant was collected and its Evans blue absorbance (at 610 nm) was measured using a microplate reader (MRX-TC; Dynex Technology, Chantilly, Virginia).

*Statistical analysis*. All data are expressed as the mean ± standard deviation (SD) from at least 3 independent experiments ($N \geqq 3$). The significance of the difference between the control and each experimental test condition was analyzed by referring to Student's *t* tests. The significance of the difference between the control and various groups and among the groups (eg, in dose-response assays) was determined using One-Way Analysis of Variance (ANOVA), followed by Duncan's new multiple range method. $P < .05$ was considered statistically significant.

## RESULTS

### *Characteristics of Gold Particles*

TEM images of gold particles are shown in Figures 1A and 1B. Quantitative measurements, shown as histograms, revealed that the average particle sizes of Au-NPs and Au-MPs were 40 ± 1 and 637 ± 9 nm, respectively. Au-NPs were observed as dispersed, unaggregated primary particles, and they showed a peak absorbance (the so-called localized surface plasmon resonance) between the wavelengths of 500 and 550 nm (Supplementary Fig. 1A). By contrast, the Au-MPs morphologically appeared as compacted crystals, and in most fields, Au-MPs formed aggregates, which resulted in an absorbance-spectrum shift to the far-red region (Supplementary Fig. 1B). The particle-size distributions measured using the DLS method are shown in Figures 1C and 1D. The average zeta potentials of Au-NP and Au-MP suspensions were −12.2 ± 0.7 and −21.0 ± 3.7 mV, respectively (Supplementary Fig. 2).

### *Effects of Au-NPs on Cell Viability*

HUVEC and GBM 8401 cultures were incubated with Au-NPs (or Au-MPs) for 24 h and then their viability was measured. In the Au-NP-treatment groups, at concentrations up to 100 μg/ml, the viability levels (% relative to control) of HUVECs and GBM 8401 cells were 90.1 ± 0.4 and 89.7 ± 1.3, respectively, whereas cell viability remained unaffected in cultures treated with Au-MPs (Supplementary Table 2). The Au-NPs and Au-MPs used in this study were neither genotoxic (*in vivo* micronucleus assay) nor mutagenic (Ames test) (Supplementary Table 3).

### *Au-NPs Reduced TJ Protein Expression, Decreased Endothelial TJ Integrity, and Increased Paracellular Permeability in Treated HUVECs*

The paracellular permeability of HUVECs treated with Au-NPs (or Au-MPs) was measured using FITC-labeled dextrans. As compared with the tracer flux of the control group, no marked changes in the flux were observed in Au-MP-treated HUVECs; by contrast, in cells treated with Au-NPs (50 μg/ml), we measured an increase in the flux of 40- and 70-kDa FITC-dextrans (Fig. 2A). The normalized TEER of the HUVEC monolayer was reduced from 34.3 ± 1.5 to 23.7 ± 1.8 $\Omega \cdot cm^2$ after Au-NP treatment (50 μg/ml; $n = 5$), whereas there was no significant reduction in the TEER of the HUVEC monolayer exposed to Au-MPs (37.1 ± 1.4 $\Omega \cdot cm^2$; $n = 4$).

Next, to examine TJ integrity, we performed immunofluorescence staining for ZO-1. Unlike in control cells, in cells treated with $H_2O_2$ (500 μM), discontinuous or intermittent ZO-1-positive strands displaying intercellular gaps were observed, which suggested that the TJ structure was damaged. These intercellular gaps were also clearly detected in HUVECs treated with Au-NPs (50 μg/ml), but the continuity of the ZO-1-positive strands was retained in HUVECs treated with Au-MPs (Fig. 2B).

We next performed Western blotting to analyze changes in the levels of AJ and TJ proteins. In Au-MP-treated HUVECs, no changes were detected in the levels of either AJ proteins (VE-cadherin and β-catenin) or TJ proteins (occludin, JAM-1, and claudin-5). However, treatment with Au-NPs (10, 50, and 100 μg/ml) markedly diminished the expression of occludin, JAM-1, and claudin-5 in HUVECs, but not that of VE-cadherin and β-catenin (Fig. 3A and Supplementary Fig. 3). The expression of occludin, JAM-1, and claudin-5 began to decrease in a statistically significant manner at 12 h after treatment, and this reduction in expression persisted for at least 48 h (Fig. 3B). We speculated that the Au-NP-induced increase in paracellular permeability and impairment of TJ tightness might have resulted from the reduction in TJ protein expression.

In contrast to Au-NP treatment, which caused a downregulation of TJ proteins, treatment with aggregates of Au-NPs exerted no effects on these proteins; this suggested that the

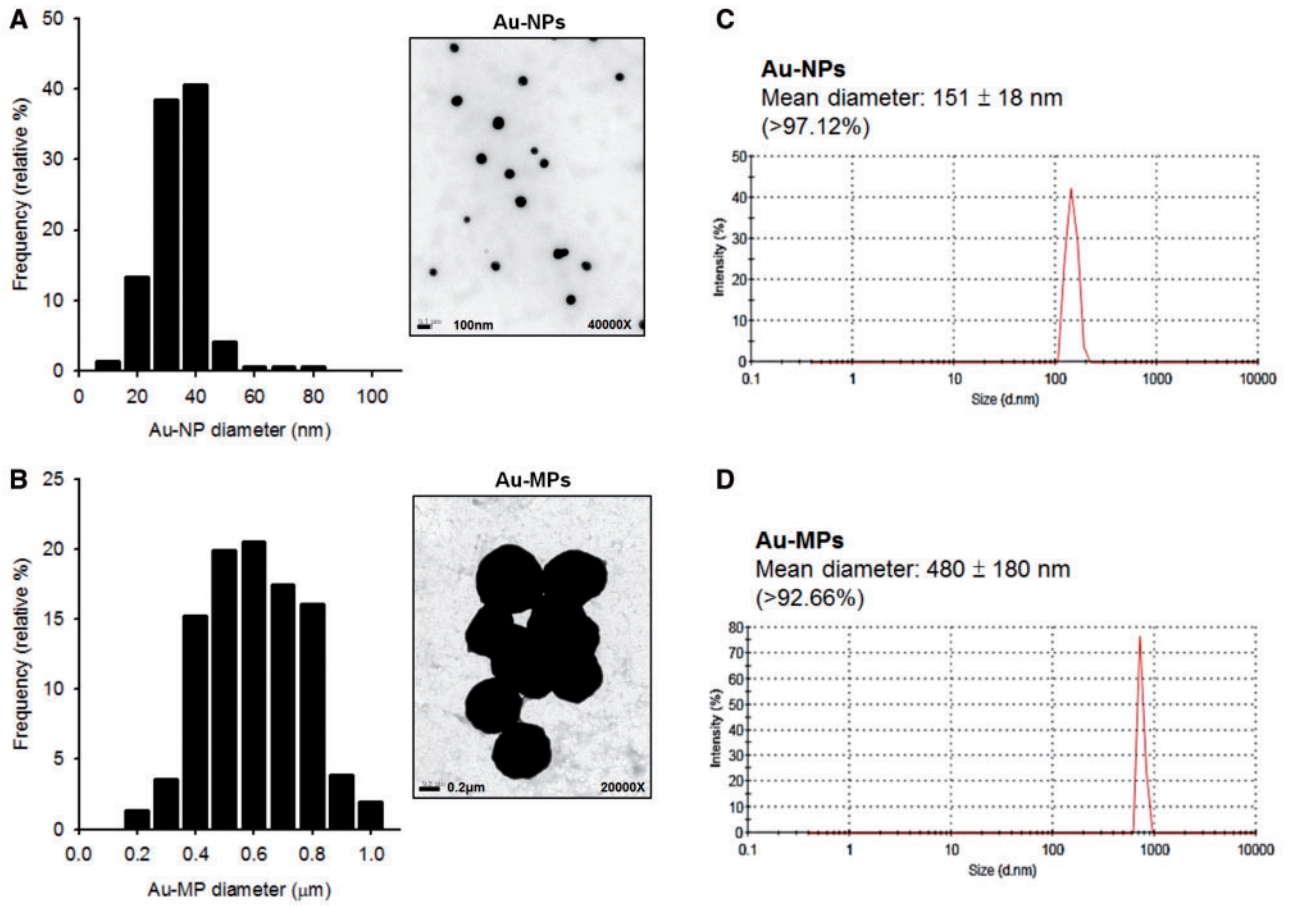


FIG. 1. Size and morphology of gold particles. A, B, Representative TEM images and Gaussian size-distribution histograms of Au-NPs (A) and Au-MPs (B) used in this study. Au-NPs were observed as primary particles featuring diameters of <100 nm (average diameter, 40 ± 1 nm), whereas Au-MPs were compacted crystals that displayed at least one external dimension of >100 nm (average diameter, 637 ± 9 nm). The aggregation of Au-MPs was found in most fields. C, D, The particle-size distribution was measured by means of DLS. The percentage and intensity-weighted average hydrodynamic diameters of Au-NPs (C) and Au-MPs (D) are shown. The gold particles were suspended in PBS. The intensity-weighted average hydrodynamic diameter of Au-NPs dispersed in cell culture medium was 153 ± 5 nm, which did not differ markedly from the diameter of Au-NPs dispersed in PBS.

downregulation of TJ proteins was caused by nano-sized Au primary particles (Supplementary Fig. 4).

### *Au-NP-Mediated TJ Protein Downregulation Was Specific to Endothelial Cells*

In addition to the permeability of the endothelial barrier, the permeability of the epithelial barrier also depends on TJ organization. However, we observed that Au-NPs induced no changes in occludin and JAM-1 protein levels in human intestinal epithelial cells (HCT-116 and Caco-2) or human brain malignant glioma GBM 8401 cells (Supplementary Fig. 5). These data revealed that Au-NP treatment downregulated TJ proteins specifically in endothelial cells.

### *Au-NP-Mediated Degradation of TJ Proteins Was Regulated Posttranscriptionally*

The mRNAs levels of VE-cadherin, β-catenin, ZO-1, occludin, JAM-1, and claudin-5 were not distinct in control HUVECs and HUVECs treated with either Au-NPs or Au-MPs (Fig. 4A and Supplementary Fig. 6). By contrast, in cells co-incubated with the 26 S proteasome inhibitor MG-132 (10 μM) and Au-NPs for 4 h, Au-NP-mediated TJ protein degradation was completely rescued (Fig. 4B), which suggested that Au-NP-induced degradation of TJ proteins was regulated by the 26 S proteasome pathway.

Under certain pathological conditions, matrix metalloproteinases (MMPs), especially MMP-9, have been shown to degrade occludin and claudin-5 and play a critical role in BBB failure (Chen *et al.*, 2009). However, in this study, we detected no marked changes in the mRNA levels of MMPs (MMP-1, -2, -9, -10, -11, and -14) after treatment with Au-NPs (or Au-MPs). Moreover, no clear changes were detected in the levels of either pro-MMP-9 or cleaved MMP-9 (Supplementary Fig. 7). These data excluded the involvement of MMPs in Au-NP-mediated TJ protein degradation.

### *Au-NPs Inhibited PKCζ Kinase Maturation and Accelerated TJ Protein Degradation*

Members of the PKC family are widely recognized to regulate the TJ barrier function. However, distinct PKC isoforms function in different tissues and play diverse roles in regulating the maintenance of cell junctions. All PKC isoforms undergo a kinase maturation process requiring phosphorylation in their catalytic domain, such as phosphorylation of Thr-497 in PKCα and Thr-560 in PKCζ (Hirai and Chida, 2003). We found that in Au-NP-treated cells, the levels of the phosphorylated form of PKCζ (Thr-560) were decreased in both time- and concentration-dependent manners (Fig. 5A and Supplementary Fig. 8A). However, the levels of the phosphorylated/non-phosphorylated

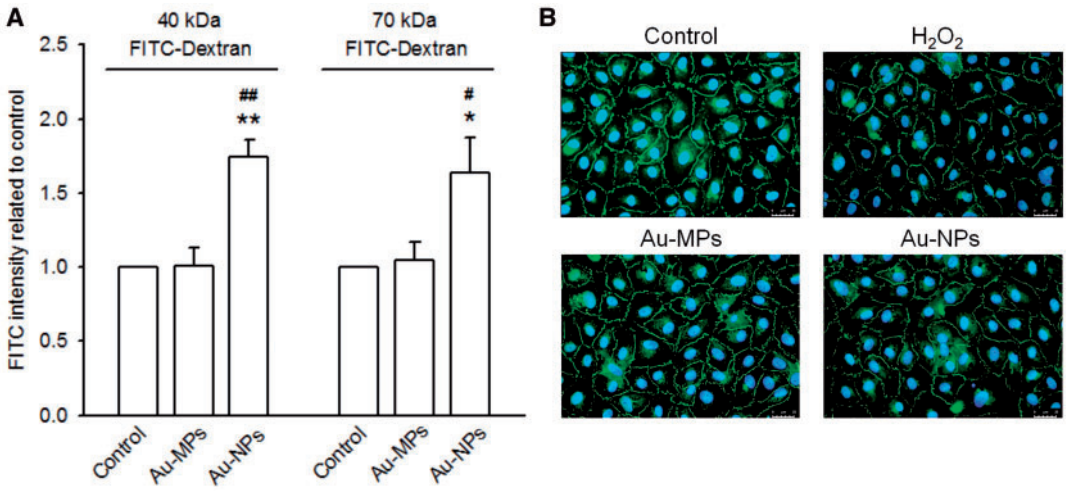


FIG. 2. Au-NP treatment diminished endothelial TJ integrity and increased paracellular permeability. A, Paracellular tracer-flux assays were performed using postconfluent HUVEC monolayers, as described in "Materials and Methods" section. Treatment with Au-NPs (50 μg/ml, 24 h) caused an increase in the paracellular permeability of FITC-dextrans (molecular masses, 40 and 70 kDa); results from 3 independent experiments are shown ($N = 3$). $^{*}P < .05$ and $^{**}P < .01$: significant differences relative to control; $^{\#}P < .05$ and $^{\#\#}P < .01$: relative to the Au-MP-treatment group. B, Photographs showing immunofluorescence staining for ZO-1 (green). The nuclei were counterstained with DAPI (blue fluorescence), and $H_2O_2$ (500 μM, 30-min treatment) was used as the positive control. Treatment with either $H_2O_2$ or Au-NPs (50 μg/ml, 24 h) caused the formation of discontinuous ZO-1-positive strands containing intercellular gaps, suggesting that TJs were damaged. Au-MP treatment did not affect TJ integrity. Representative images from 4 independent experiments are shown ($N = 4$). The scale bar on this drawing represents a length of 25 μm. Sterile water (10‰) was used in the control treatment.

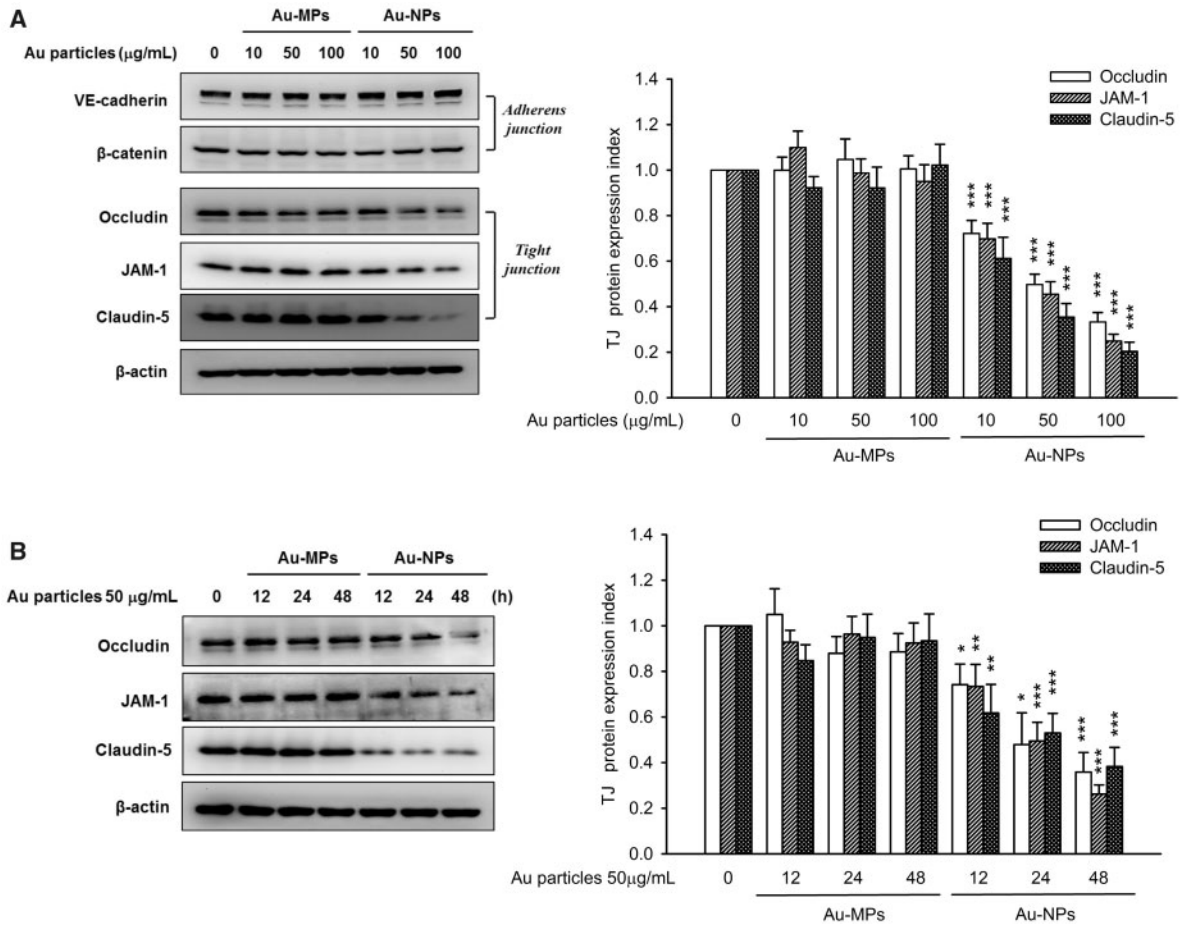


FIG. 3. Effects of Au-NPs on the expression of AJ and TJ proteins in HUVECs. The figure shows representative images and quantified data of Western blots demonstrating the changes in the amounts of AJ and TJ proteins in HUVECs treated with Au-NPs (or Au-MPs). A, The expression of occludin, JAM-1, and claudin-5 was downregulated in HUVECs treated with Au-NPs (10, 50, 100 μg/ml; 24 h), but not in cells treated with Au-MPs. Neither Au-NPs nor Au-MPs affect the expression of VE-cadherin and β-catenin. B, Au-NP treatment downregulated the expression of occludin, JAM-1, and claudin-5 in a time-dependent manner, but treatment with Au-MPs did not alter the expression of these proteins. $^{*}P < .05$, $^{**}P < .01$, and $^{***}P < .001$: significant differences relative to control ($N = 5$–7). Sterile water (10‰) was used in the control treatment.

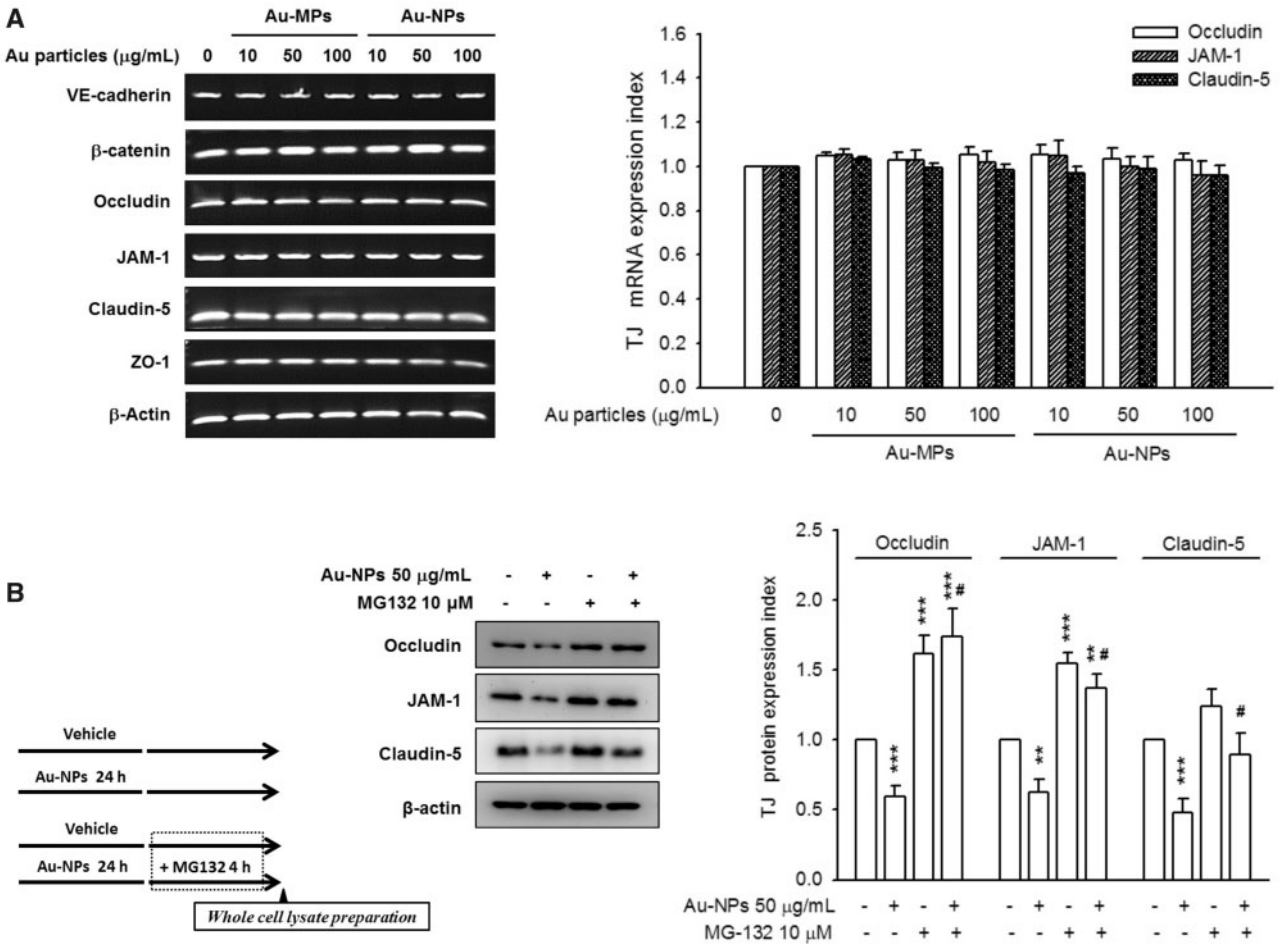


FIG. 4. Au-NP-mediated TJ protein degradation was regulated posttranscriptionally. A, Treatment of HUVECs with Au-NPs (or Au-MPs) altered the mRNA expression of neither AJ proteins (VE-cadherin and β-catenin) nor TJ proteins (occludin, JAM-1, claudin-5, and ZO-1). B, HUVECs were co-incubated with Au-NPs (50 μg/ml) and the 26 S proteasome inhibitor MG132 (10 μM). Au-NP-mediated degradation of TJ proteins could be fully rescued by MG132, suggesting the involvement of 26 S proteasome in Au-NP-dependent TJ protein degradation. $^{*}P < .05$, $^{**}P < .01$, and $^{***}P < .001$: significant differences relative to control ($N = 4$); $^{\#}P < .05$: relative to the Au-NP-treatment group. The solvent control treatment was 10‰ sterile water (A) or 1‰ DMSO (B).

forms of PKCα Src, FAK, and Rac1 remained unaffected by Au-NP treatment (Supplementary Fig. 8B). Gö6983, a broad-spectrum PKC inhibitor, not only inhibited PKCζ Thr-560 phosphorylation (30-min treatment), but also downregulated the expression of TJ proteins (24-h treatment). Moreover, following pretreatment/co-incubation with Gö6983, Au-NP-mediated TJ protein degradation was enhanced (Fig. 5B), and immunofluorescence labeling confirmed that the TJ structure at the cell borders was disassembled (Supplementary Fig. 9). These data suggested the requirement of PKCζ activation for maintaining TJ integrity.

The results of complementary experiments showed that arachidonic acid (50 μM), an activator of PKCζ, induced PKCζ Thr-560 phosphorylation (30-min treatment), but did not affect TJ protein expression (24-h treatment). However, following pretreatment/co-incubation with arachidonic acid, Au-NP-mediated TJ protein degradation was partially rescued (Fig. 5C), as was the integrity of TJs at the cell border (Supplementary Fig. 9). These data indicated that Au-NPs might induce TJ disassembly in a PKCζ-dependent manner and lead to the degradation of TJ proteins.

*Au-NP Treatment Reduced the Threonine Phosphorylation of Occludin and ZO-1.* Hyper-phosphorylation on Ser and Thr residues of ZO-1 and occludin is necessary for occludin/ZO-1 association (Rao, 2009). The results of immunoprecipitation experiments showed that threonine phosphorylation of captured ZO-1 and occludin was markedly lower after treatment with Au-NPs than after treatment with Au-MPs. Moreover, Au-NP treatment reduced the occludin/ZO-1 association in co-immunoprecipitation assays (Figs. 6A and 6B), and the amounts of ZO-1 and occludin immunoprecipitated by the p-Thr capture antibody were clearly decreased after Au-NP treatment, but were unaffected in the control and Au-MP-treatment groups (Fig. 6C).

*Au-NPs Decreased TJ Integrity of BMEC Monolayers and Enhanced BBB Permeability In Vivo.* We validated the Au-NP-induced reduction in endothelial TJ integrity by using isolated mouse BMECs. Immunofluorescence staining showed that ZO-1 and occludin were expressed mainly on the cell border and that the staining appeared as continuous strands in the control and Au-MP-treatment groups. However, after treatment with Au-NPs or $H_2O_2$, these strands appeared discontinuous and the fluorescence became scattered (Fig. 7A). Lastly, we examined the effect of Au-NPs on BBB permeability by means of Evans blue extravasation *in vivo*. In control mice, at 2 h after intravenous injection of Evans blue, the dye was not detected in the brain. By contrast, in mice that were administered Au-NPs (12.5 and 25 mg/kg b.w., i.v.), blue staining of the brain was evident at 24 and 48 h after

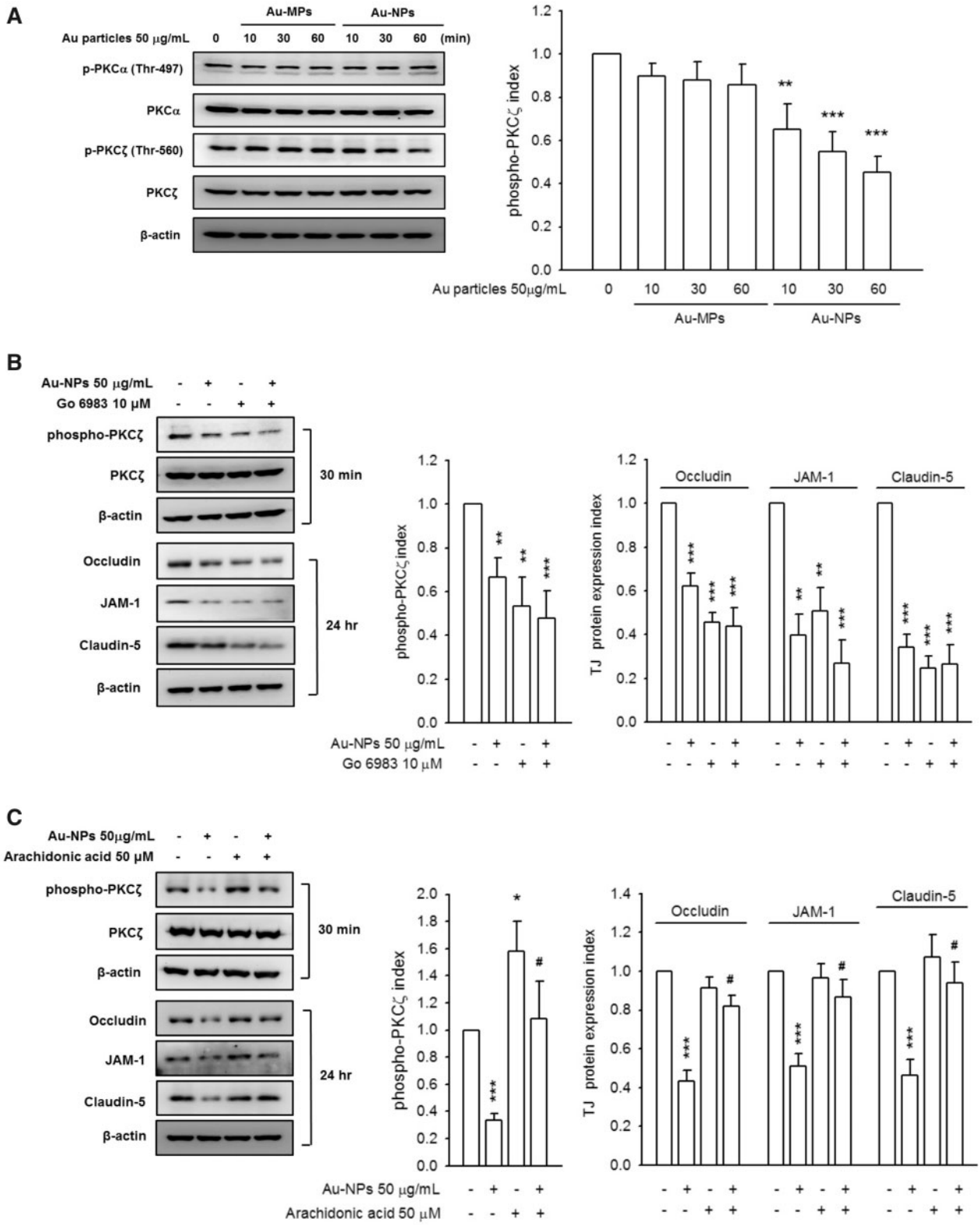


**FIG. 5.** Basal PKCζ activation was required for TJ integrity. A, Representative images showing that the phosphorylation of PKCζ, but not PKCα was decreased over time in HUVECs treated with Au-NPs (50 μg/ml; 10, 30, and 60 min). Neither PKCζ nor PKCα responded to Au-MP treatment. B, Similar to treatment with Au-NPs, treatment with the PKCζ inhibitor Gö6983 (10 μM) caused not only PKCζ dephosphorylation (Thr-560), but also TJ protein degradation. Moreover, the extent of Au-NP-mediated TJ protein degradation was increased when cells were pretreated/co-incubated with Gö6983. C, Treatment with the PKCζ activator arachidonic acid (50 μM) increased PKCζ phosphorylation, but did not markedly alter the expression of TJ proteins. However, Au-NP-mediated TJ protein degradation was partially rescued following pretreatment/co-incubation with arachidonic acid. These data highlight the requirement of a basal level of PKCζ activation for TJ integrity: A reduction in PKCζ activation leads to TJ instability and TJ protein degradation. $^{*}P < .05$, $^{**}P < .01$, and $^{***}P < .001$: significant differences relative to control ($N = 4–6$); $^{\#}P < .05$: relative to the Au-NP-treatment group. The solvent control treatment was 10‰ sterile water (A), 1‰ DMSO (B), or 2‰ DMSO (C).

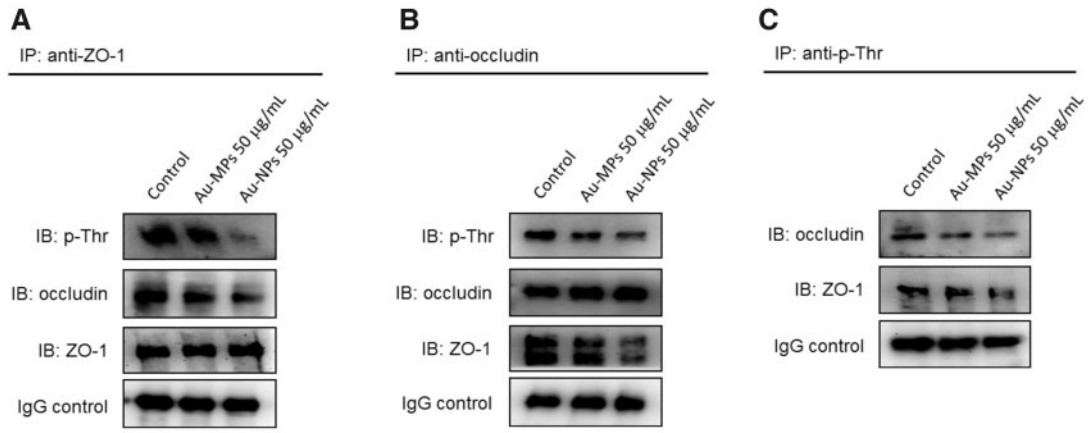


FIG. 6. Au-NP treatment reduced threonine phosphorylation on ZO-1 and occludin. Proteins were immunoprecipitated using anti-ZO-1, anti-occludin, or anti-phospho-threonine (p-Thr) antibodies, as described in "Materials and Methods" section. Representative images from 4 independent experiments are shown ($N = 4$); IgG was used as the loading control. A, In HUVECs treated with Au-NPs (50 μg/ml; 12 h), threonine phosphorylation of captured ZO-1 and the associated occludin was clearly lower than the corresponding phosphorylation levels in the control sample. However, Au-MP treatment did not affect the phosphorylation of these proteins. B, When co-immunoprecipitation assays were performed using the anti-occludin capture antibody, the threonine phosphorylation of captured occludin and the associated ZO-1 was once again found to be decreased following Au-NP treatment; no changes were observed in the control and Au-MP-treatment groups. C, Lastly, in immunoprecipitates obtained using the anti-p-Thr capture antibody, the levels of ZO-1 and occludin were diminished following Au-NP treatment, whereas they were unaffected by Au-MP treatment.

dosing. Quantification of the data showed that the Evans blue content was increased in a statistically significant manner at 24 h after administration of the 2 doses of Au-NPs (Fig. 7B).

## DISCUSSION

Adjoining cells closely adhere to each other through 3 intercellular junctions, AJs, TJs, and gap junctions. Specifically, AJs and TJs are responsible for regulating paracellular permeability, which is tightly controlled in the endothelium. Molecules such as vascular endothelial growth factor (VEGF) (Gavard and Gutkind, 2006), ethanol (Xu *et al.*, 2012), and actin-depolymerizing agents (Millan *et al.*, 2010), which disturb the stability of the VE-cadherin/β-catenin complex or AJs, typically damage the endothelial barrier (Harris and Nelson, 2010). The presence of AJs is also required for stabilizing TJ formation (Taddei *et al.*, 2008). In this study, we found that Au-NP treatment increased endothelial barrier permeability *in vitro*, but it did not affect the expression of VE-cadherin and β-catenin; this suggests that paracellular permeability is more likely regulated by TJs than by AJs.

TJ complexes contain a wide spectrum of proteins, and among these, occludin, claudins, and JAMs are integral membrane proteins. One or more claudins, which share high sequence identity but are differentially expressed in various tissues, constitute the core of the TJ complexes. Ochratoxin A (McLaughlin *et al.*, 2004), human chorionic gonadotropin (Rodewald *et al.*, 2009), VEGF (Argaw *et al.*, 2009), and deoxynivalenol (Pinton *et al.*, 2009), which cause the removal of specific claudins from TJs, have been shown to allow claudin pore formation and ion permeability. Claudin-5 is expressed specifically by endothelial cells (Gonçalves *et al.*, 2013), and an *in vitro* study showed that overexpressed claudin-5 became concentrated at endothelial cell borders, where it interacted with ZO-1 and ensured tight contact between cells (Umeda *et al.*, 2006). In the vascular tree, the levels of occludin expression were reported to determine endothelial barrier permeability (Hirase *et al.*, 1997). Like claudins, occludin binds directly to ZO-1 through its C-terminal domain, and disruption of the occludin/ZO-1 interaction (especially using an occludin mutant containing a C-terminal deletion) was shown to cause the removal of occludin from TJs (Balda *et al.*, 1996). In the case of JAMs, humans express 3 isoforms, and the isoform JAM-1, which is universally expressed in the epithelium and the endothelium, also functionally interacts with ZO-1 and contributes to TJ (and BBB) tightness (Yeung *et al.*, 2008). In this study, Au-NP treatment diminished the integrity of TJs and the expression of TJ proteins, which suggests that endothelial paracellular permeability is increased as a result of Au-NP-mediated TJ protein degradation and TJ leakiness.

TJ integrity can be regulated by various factors such as inflammatory cytokines, growth factors, oxidative stress, bacterial toxins (Rao, 2008), and nanoparticles (Brun *et al.*, 2014; Trickler *et al.*, 2014). Treatment with Cu-NPs, Ag-NPs, and $TiO_2$-NPs has been reported to increase the generation of free radicals (Sarkar *et al.*, 2014) and the release of inflammatory cytokines (Marano *et al.*, 2011) and to increase paracellular permeability (Brun *et al.*, 2014; Trickler *et al.*, 2014). Both free radicals and inflammatory cytokines are widely recognized to induce TJ damage, and thus the nanoparticles might impair TJ structure and function by elevating these active factors. However, because no available evidence suggests a correlation between Au-NP exposure and the formation of free radicals or inflammatory cytokines (Trickler *et al.*, 2011), a novel mechanism might be involved in Au-NP-mediated TJ regulation.

As mentioned earlier in this section, the interaction between ZO-1 and occludin (and also JAM-1 and claudin-5) helps stabilize the TJ structure. Increasing evidence indicates that the phosphorylation of occludin and ZO-1 can regulate TJ assembly or disassembly (Bazzoni and Dejana, 2004). This regulation has been shown to depend mainly on the kinases/phosphatases involved and the residues/positions phosphorylated (Rao, 2009). For example, occludin phosphorylation on Thr-424/438 (by PKCζ) appears to be required for TJ assembly (Jain *et al.*, 2011). However, phosphorylation on Tyr and Ser residues typically attenuates occludin/ZO-1 complex formation (Elias *et al.*, 2009; Murakami *et al.*, 2012; Raleigh *et al.*, 2011; Yamamoto *et al.*, 2008). In this study, treatment of endothelial cells with Au-NPs caused a reduction in the threonine phosphorylation of ZO-1 and occludin and diminished the ZO-1/occludin interaction.

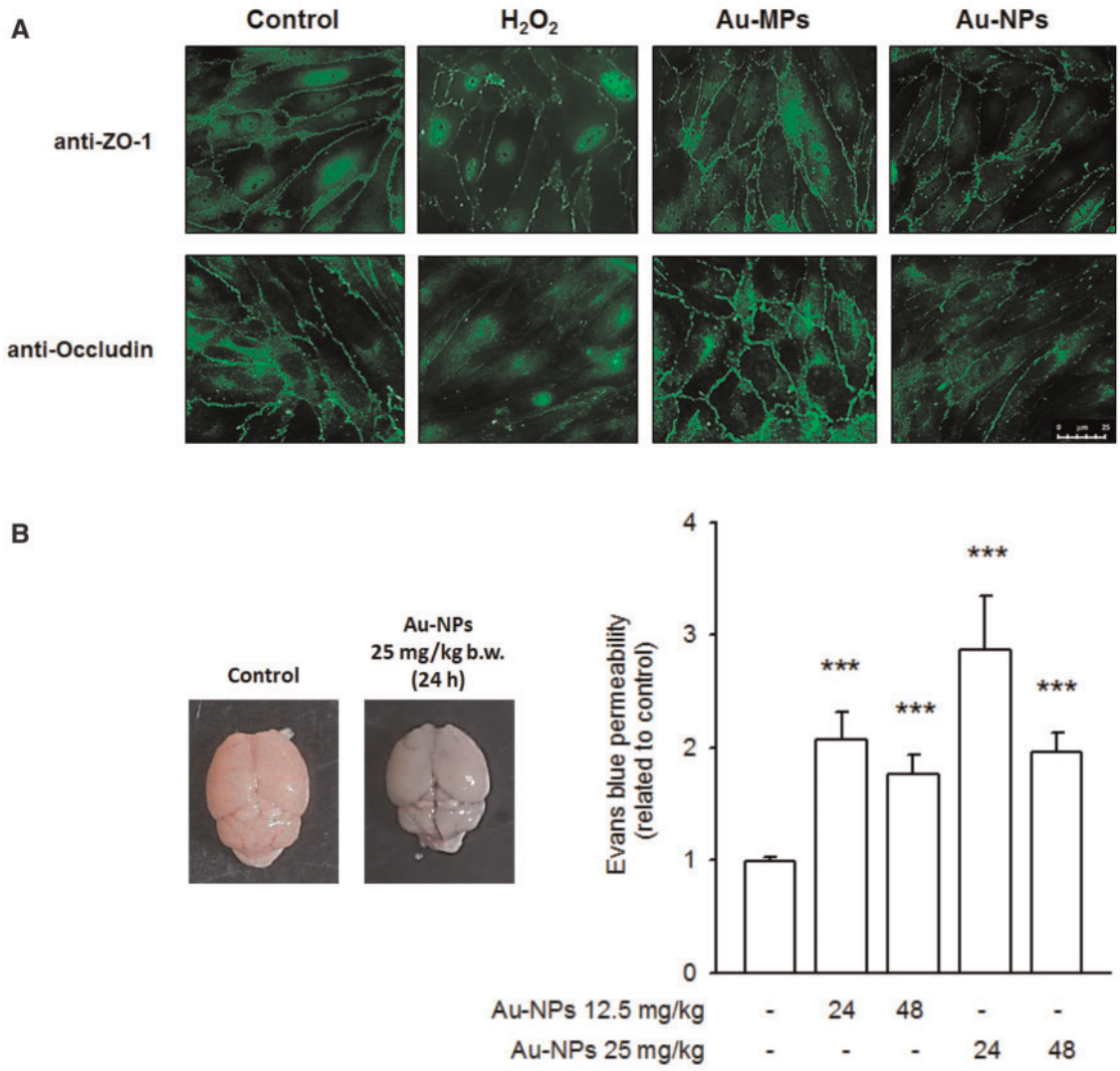


**FIG. 7.** Au-NPs decreased the TJ integrity of BMEC monolayers and enhanced BBB permeability *in vivo*. A, Mouse BMECs were isolated and cultured as described in Supplementary Information. The images show the green immunofluorescence of the stained ZO-1 (upper panel) or occludin (lower panel). In control and Au-MP-treatment groups, both ZO-1 and occludin were stained as continuous strands on the cell surface. However, these strands became discontinuous and the fluorescence became scattered after treatment with Au-NPs (50 μg/ml, 24 h) or $H_2O_2$ (500 μM, 30 min). These data suggested that the Au-NP-induced damage of TJs can be validated in mouse BMECs. Representative images of 3 independent experiments are shown ($N = 3$). B, Evaluation of BBB permeability *in vivo*. Mice were injected with a single dose of Au-NPs (12.5 or 25 mg/kg b.w., i.v.) and then were subjected to Evans blue extravasation at 24 and 48 h after dosing, as described in "Materials and Methods" section. The paracellular transport of Evans blue dye from the circulation into the brain tissues was higher in mice that had received Au-NPs than in the mice that were injected with saline (control). Kinetic and biodistribution studies (Khlebtsov and Dykmana, 2011) indicate that the blood concentration of Au-NPs rapidly declines initially (at 4 h after dosing), and that this is followed by a gradual decrease. Thus, the estimated concentration of Au-NPs in mice treated with 25 mg/kg Au-NPs might fall to 7.5–10 μg/g (at 4 h after dosing; 30–40% of the given dose), which is close to the low dose applied *in vitro* (10 μg/ml). ***$P < .001$: significant difference relative to control ($N = 5$).

Most previous studies indicate that PKCs play a central role in TJ regulation and exert both stimulatory and inhibitory effects. In this study, PKCα did not respond to Au-NPs, but PKCζ was inactivated after Au-NP treatment. Stimuli such as TNF-α (Aveleira *et al.*, 2010), VEGF (Titchenell *et al.*, 2012), hyperglycemia (Omri *et al.*, 2013), and hypoxia (Willis *et al.*, 2010), which induce the hyper-activation of PKCζ, subsequently compromise TJ complexes. Inhibition of PKCζ hyper-activation restores not only the integrity of TJs, but also their barrier functions. Conversely, PKCζ can also serve as a direct substrate for phosphoinositide-dependent protein kinase 1 and PI-3 kinase signaling. Moreover, PKCζ is recruited to the membrane and is constitutively active in the absence of agonist stimulation (Newton, 2010). Membrane-recruited PKCζ directly interacts with occludin, induces the phosphorylation of occludin on Thr-424/438 residues and positively regulates TJ assembly (Balda *et al.*, 1993). In this study, co-incubation of cells with Au-NPs and a PKCζ inhibitor (Gö6983) or activator (arachidonic acid) exacerbated or partly alleviated Au-NP-mediated TJ protein degradation, respectively. These data suggested that a basal level of PKCζ activation was crucial for endothelial TJ assembly, and that PKCζ inhibition caused by Au-NP treatment led to a disruption of barrier function.

Three barriers exist between the blood and the brain: the BBB, the blood-cerebrospinal fluid barrier (BCSFB), and the arachnoid barrier. In the arachnoid barrier, a multi-layered epithelium containing TJs is present, whereas in the BCSFB, capillary endothelial cells are fenestrated, and TJs are formed

between epithelial cells at the apical surface (the CSF-facing surface). Thus, the BCSFB and the arachnoid barrier contain epithelial TJs, rather than endothelial TJs (Abbott, 2013; Engelhardt and Sorokin, 2009). Our data suggested that Au-NP-mediated downregulation of TJ proteins occurred in endothelial cells, but not in epithelial cells. Based on the results of both *in vitro* and *in vivo* assays, we conclude that Au-NP-induced Evans dye diffusion in brain might result from endothelial TJ damage and BBB leakiness.

In this study, we first determined that Au-NPs increased endothelial paracellular permeability *in vitro* and enhanced BBB permeability *in vivo*. Our results also provided an enhanced understanding of the mechanism of action of Au-NPs: the nanoparticles inactivated PKCζ, suppressed threonine phosphorylation on occludin and ZO-1, and perturbed occludin/ZO-1 complex formation, and thus caused TJ disassembly and TJ protein degradation. These results demonstrated that Au-NPs, which hold great potential for use in biomedicine, can substantially increase endothelial permeability and thereby enhance the transport of other molecules, xenobiotics, or pathogens into the brain. This double-edged-sword effect of Au-NPs must continue to receive attention and must be investigated further in future studies.

## SUPPLEMENTARY DATA

Supplementary data are available online at http://toxsci.oxfordjournals.org/.

## ACKNOWLEDGMENTS

This study was financed in part by the grants TMU101-AE1-B46 (funded by Taipei Medical University), DOH102-FDA-31103 (funded by the Food and Drug Administration, Ministry of Health and Welfare, Taiwan), and MOST 103-2320-B-038-033 (funded by the Ministry of Science and Technology, Taiwan).
The authors have no conflicts of interest to declare.

## REFERENCES

Abbott, N. J. (2013). Blood-brain barrier structure and function and the challenges for CNS drug delivery. *J. Inherit. Metab. Dis.* **36**, 437–449.

Abbott, N. J., Rönnbäck, L., and Hansson, E. (2006). Astrocyte-endothelial interactions at the blood-brain barrier. *Nat. Rev. Neurosci.* **7**, 41–53.

Argaw, A. T., Gurfein, B. T., Zhang, Y., Zameer, A., and John, G. R. (2009). VEGF-mediated disruption of endothelial CLN-5 promotes blood-brain barrier breakdown. *Proc. Natl Acad. Sci. U. S. A.* **106**, 1977–1982.

Aveleira, C. A., Lin, C. M., Abcouwer, S. F., Ambrósio, A. F., and Antonetti, D. A. (2010). TNF-α signals through PKCζ/NF-κB to alter the tight junction complex and increase retinal endothelial cell permeability. *Diabetes* **59**, 2872–2882.

Balda, M. S., Gonzalez-Mariscal, L., Matter, K., Cereijido, M., and Anderson, J. M. (1993). Assembly of the tight junction: the role of diacylglycerol. *J. Cell Biol.* **123**, 293–302.

Balda, M. S., Whitney, J. A., Flores, C., Gonzalez, S., Cereijido, M., and Matter, K. (1996). Functional dissociation of paracellular permeability and transepithelial electrical resistance and disruption of the apical-basolateral intramembrane diffusion barrier by expression of a mutant tight junction membrane protein. *J. Cell Biol.* **134**, 1031–1049.

Bazzoni, G., and Dejana, E. (2004). Endothelial cell-to-cell junctions: molecular organization and role in vascular homeostasis. *Physiol. Rev.* **84**, 869–901.

Beese, M., Wyss, K., Haubitz, M., and Kirsch, T. (2010). Effect of cAMP derivates on assembly and maintenance of tight junctions in human umbilical vein endothelial cells. *BMC Cell Biol.* **11**, 68.

Bowman, P. D., Ennis, S. R., Rarey, K. E., Betz, A. L., and Goldstein, G. W. (1983). Brain microvessel endothelial cells in tissue culture: a model for study of blood-brain barrier permeability. *Ann. Neurol.* **14**, 396–402.

Brun, E., Barreau, F., Veronesi, G., Fayard, B., Sorieul, S., Chanéac, C., Carapito, C., Rabilloud, T., Mabondzo, A., Herlin-Boime, N., *et al.* (2014). Titanium dioxide nanoparticle impact and translocation through ex vivo, in vivo and in vitro gut epithelia. *Part. Fibre Toxicol.* **11**, 13.

Chen, F., Ohashi, N., Li, W., Eckman, C., and Nguyen, J. H. (2009). Disruptions of occludin and claudin-5 in brain endothelial cells in vitro and in brains of mice with acute liver failure. *Hepatology* **50**, 1914–1923.

Dodane, V., and Kachar, B. (1996). Identification of isoforms of G proteins and PKC that colocalize with tight junctions. *J. Membr. Biol.* **149**, 199–209.

Elias, B. C., Suzuki, T., Seth, A., Giorgianni, F., Kale, G., Shen, L., Turner, J. R., Naren, A., Desiderio, D. M., and Rao, R. (2009). Phosphorylation of Tyr-398 and Tyr-402 in occludin prevents its interaction with ZO-1 and destabilizes its assembly at the tight junctions. *J. Biol. Chem.* **284**, 1559–1569.

Engelhardt, B., and Sorokin, L. (2009). The blood–brain and the blood-cerebrospinal fluid barriers: function and dysfunction. *Semin. Immunopathol.* **31**, 497–511.

Gavard, J., and Gutkind, J. S. (2006). VEGF controls endothelial-cell permeability by promoting the beta-arrestin-dependent endocytosis of VE-cadherin. *Nat. Cell Biol.* **8**, 1223–1234.

Gonçalves, A., Ambrósio, A. F., and Fernandes, R. (2013). Regulation of claudins in blood-tissue barriers under physiological and pathological states. *Tissue Barriers* **1**, e24782.

Harris, E. S., and Nelson, W. J. (2010). VE-cadherin: at the front, center, and sides of endothelial cell organization and function. *Curr. Opin. Cell. Biol.* **22**, 651–658.

He, F., Yin, F., Omran, A., Yang, L. F., Xiang, Q. L., and Peng, J. (2012). PKC and RhoA signals cross-talk in *Escherichia coli* endotoxin induced alterations in brain endothelial permeability. *Biochem. Biophys. Res. Commun.* **425**, 182–188.

Hirai, T., and Chida, K. (2003). Protein kinase Czeta (PKCzeta): activation mechanisms and cellular functions. *J. Biochem.* **133**, 1–7.

Hirase, T., Staddon, J. M., Saitou, M., Ando-Akatsuka, Y., Itoh, M., Furuse, M., Fujimoto, K., Tsukita, S., and Rubin, L. L. (1997). Occludin as a possible determinant of tight junction permeability in endothelial cells. *J. Cell Sci.* **110**, 1603–1613.

Jain, S., Suzuki, T., Seth, A., Samak, G., and Rao, R. (2011). PKCζ phosphorylates occludin and promotes assembly of epithelial tight junctions. *Biochem. J.* **437**, 289–299.

Khlebtsov, N., and Dykmana, L. (2011). Biodistribution and toxicity of engineered gold nanoparticles: a review of in vitro and in vivo studies. *Chem. Soc. Rev.* **40**, 1647–1671.

Li, C. H., Liao, P. L., Shyu, M. K., Liu, C. W., Kao, C. C., Huang, S. H., Cheng, Y. W., and Kang, J. J. (2012). Zinc oxide nanoparticles-induced intercellular adhesion molecule 1 expression requires Rac1/Cdc42, mixed lineage kinase 3, and c-Jun N-terminal kinase activation in endothelial cells. *Toxicol. Sci.* **126**, 162–172.

Liu, P., Woda, M., Ennis, F. A., and Libraty, D. H. (2009). Dengue virus infection differentially regulates endothelial barrier function over time through type I interferon effects. *J. Infect. Dis.* **200**, 191–201.

Marano, F., Hussain, S., Rodrigues-Lima, F., Baeza-Squiban, A., and Boland, S. (2011). Nanoparticles: molecular targets and cell signalling. *Arch. Toxicol.***85**, 733–741.

Mayanglambam, A., Bhavanasi, D., Vijayan, K. V., and Kunapuli, S. P. (2011). Differential dephosphorylation of the protein kinase C-zeta (PKCζ) in an integrin αIIbβ3-dependent manner in platelets. *Biochem. Pharmacol.* **82**, 505–513.

McLaughlin, J., Padfield, P. J., Burt, J. P. H., and O'Neill, C. A. (2004). Ochratoxin A increases permeability through tight junctions by removal of specific claudin isoforms. *Am. J. Physiol. Cell Physiol.* **287**, C1412–C1417.

Millan, J., Cain, R. J., Reglero-Real, N., Bigarella, C., Marcos-Ramiro, B., Fernandez-Martin, L., Correas, I., and Ridley, A. J. (2010). Adherens junctions connect stress fibres between adjacent endothelial cells. *BMC Biol.***8**, 11.

Murakami, T., Frey, T., Lin, C., and Antonetti, D. A. (2012). Protein kinase Cβ phosphorylates occludin regulating tight junction trafficking in vascular endothelial growth factor-induced permeability in vivo. *Diabetes* **61**, 1573–1583.

Newton, A. C. (2010). Protein kinase C: poised to signal. *Am. J. Physiol. Endocrinol. Metab.* **298**, E395–E402.

Omri, S., Behar-Cohen, F., Rothschild, P. R., Gélizé, E., Jonet, L., Jeanny, J. C., Omri, B., and Crisantim P. (2013). PKCζ mediates breakdown of outer blood-retinal barriers in diabetic retinopathy. *PLoS One* **8**, e81600.

Panyala, N. R., Peña-Méndez, E. M., and Havel, J. (2009). Gold and nano-gold in medicine: overview, toxicology and perspectives. *J. Appl. Biomed.***7**, 75–91.

Pinton, P., Nougayrède, J. P., Del Rio, J. C., Moreno, C., Marin, D. E., Ferrier, L., Bracarense, A. P., Kolf-Clauw, M., and Oswald, I. P. (2009). The food contaminant deoxynivalenol, decreases intestinal barrier permeability and reduces claudin expression. *Toxicol. Appl. Pharmacol.* **237**, 41–48.

Raleigh, D. R., Boe, D. M., Yu, D., Weber, C. R., Marchiando, A. M., Bradford, E. M., Wang, Y., Wu, L., Schneeberger, E. E., Shen, L., *et al.* (2011). Occludin S408 phosphorylation regulates tight junction protein interactions and barrier function. *J. Cell Biol.* **193**, 565–582.

Rao, R. (2008). Oxidative stress-induced disruption of epithelial and endothelial tight junctions. *Front. Biosci.* **13**, 7210–7226.

Rao, R. (2009). Occludin phosphorylation in regulation of epithelial tight junctions. *Ann. N. Y. Acad. Sci.* **1165**, 62–68.

Rodewald, M., Herr, D., Duncan, W. C., Fraser, H. M., Hack, G., Konrad, R., Gagsteiger, F., Kreienberg, R., and Wulff, C. (2009). Molecular mechanisms of ovarian hyperstimulation syndrome: paracrine reduction of endothelial claudin 5 by hCG in vitro is associated with increased endothelial permeability. *Hum. Reprod.***24**, 1191–1199.

Sarkar, A., Ghosh, M., and Sil, P. C. (2014). Nanotoxicity: oxidative stress mediated toxicity of metal and metal oxide nanoparticles. *J. Nanosci. Nanotechnol.* **14**, 730–743.

Stamatovic, S. M., Dimitrijevic, O. B., Keep, R. F., and Andjelkovic, A. V. (2006) .Protein kinase Calpha-RhoA cross-talk in CCL2-induced alterations in brain endothelial permeability. *J. Biol. Chem.* **281**, 8379–8388.

Taddei, A., Giampietro, C., Conti, A., Orsenigo, F., Breviario, F., Pirazzoli, V., Potente, M., Daly, C., Dimmeler, S., and Dejana, E. (2008). Endothelial adherens junctions control tight junctions by VE-cadherin-mediated upregulation of claudin-5. *Nat. Cell Biol.* **10**, 923–934.

Titchenell, P. M., Lin, C. M., Keil, J. M., Sundstrom, J. M., Smith, C. D., and Antonetti, D. A. (2012). Novel atypical PKC inhibitors prevent vascular endothelial growth factor-induced blood-retinal barrier dysfunction. *Biochem. J.* **446**, 455–467.

Trickler, W. J., Lantz, S. M., Murdock, R. C., Schrand, A. M., Robinson, B. L., Newport, G. D., Schlager, J. J., Oldenburg, S. J., Paule, M. G., Slikker, W., Jr., *et al.* (2011). Brain microvessel endothelial cells responses to gold nanoparticles: In vitro pro-inflammatory mediators and permeability. *Nanotoxicology* **5**, 479–492.

Trickler, W. J., Lantz-McPeak, S. M., Robinson, B. L., Paule, M. G., Slikker, W. Jr., Biris, A. S., Schlager, J. J., Hussain, S. M., Kanungo, J., *et al.* (2014). Porcine brain microvessel endothelial cells show pro-inflammatory response to the size and composition of metallic nanoparticles. *Drug Metab. Rev.* **46**, 224–231.

Umeda, K., Ikenouchi, J., Katahira-Tayama, S., Furuse, K., Sasaki, H., Nakayama, M., Matsui, T., Tsukita, S., and Furuse, M. (2006). ZO-1 and ZO-2 independently determine where claudins are polymerized in tight-junction strand formation. *Cell* **126**, 741–754.

Wang, P., Liu, Y., Shang, X., and Xue, Y. (2011). CRM197-induced blood-brain barrier permeability increase is mediated by upregulation of caveolin-1 protein. *J. Mol. Neurosci.* **43**, 485–492.

Willis, C. L., Meske, D. S., and Davis, T. P. (2010). Protein kinase C activation modulates reversible increase in cortical blood-brain barrier permeability and tight junction protein expression during hypoxia and posthypoxic reoxygenation. *J. Cereb. Blood Flow Metab.* **30**, 1847–1859.

Xu, M., Chen, G., Fu, W., Liao, M., Frank, J. A., Bower, K. A., Fang, S., Zhang, Z., Shi, X., and Luo, J. (2012). Ethanol disrupts vascular endothelial barrier: implication in cancer metastasis. *Toxicol. Sci.* **127**, 42–53.

Yamamoto, M., Ramirez, S. H., Sato, S., Kiyota, T., Cerny, R. L., Kaibuchi, K., Persidsky, Y., and Ikezu, T. (2008). Phosphorylation of claudin-5 and occludin by rho kinase in brain endothelial cells. *Am. J. Pathol.* **172**, 521–533.

Yeung, D., Manias, J. L., Stewart, D. J., and Nag, S. (2008). Decreased junctional adhesion molecule-A expression during blood–brain barrier breakdown. *Acta Neuropathol.* **115**, 635–642.

Zyrek, A. A., Cichon, C., Helms, S., Enders, C., Sonnenborn, U., and Schmidt, M. A. (2007). Molecular mechanisms underlying the probiotic effects of *Escherichia coli* Nissle 1917 involve ZO-2 and PKCzeta redistribution resulting in tight junction and epithelial barrier repair. *Cell Microbiol.* **9**, 804–816.